AIAA JOURNAL
Vol. 38, No. 1, January 2000

Effects of Injection Angle on Atomization of Liquid Jets in Transverse Airflow

Raymond P. Fuller,* Pei-Kuan Wu,† and Kevin A. Kirkendall‡
Taitech, Inc., Dayton, Ohio 45431
and
Abdollah S. Nejad§
U.S. Air Force Research Laboratory, Wright–Patterson Air Force Base, Ohio 45433

An experimental investigation was conducted to study and characterize the effects of injection angle on the breakup processes of turbulent liquid jets in a subsonic crossflow of air. With water as the test liquid, the injection angle, freestream Mach number, and injection velocity were varied over a wide range to provide an extensive database of experimental results. Pulsed shadowgraph photography was employed to ascertain column trajectories, column fracture locations, and near-field spray characteristics. Results indicate that column breakup behavior can be divided into two distinct regimes: aerodynamic and nonaerodynamic. Liquid column fracture locations were found to be governed by length scales, which depend on the corresponding breakup regime. For aerodynamic breakup, the column length scale was derived from the timescale for the analogous process of the aerodynamic secondary breakup of a droplet. For nonaerodynamic breakup, the column length scale was derived from the timescale for the breakup of a turbulent liquid jet issuing into a quiescent gas. A breakup regime parameter was defined to determine, based on jet operating conditions, the prevalent breakup regime and, therefore, the appropriate column length scale. Liquid column trajectories were correlated with an effective jet-to-freestream momentum flux ratio and transverse injection angle by applying a force balance and momentum analysis. Comparisons between experimental data and analytical predictions are presented and show excellent agreement in most cases.

Nomenclature

C_{ab} = constant for aerodynamic breakup
C_D = drag coefficient, $2D/\rho_\infty u_\infty^2$
C_{fb} = constant for nonaerodynamic breakup
D = aerodynamic drag force
d = injector diameter
L = liquid column length scale
l = length
M = Mach number
Oh_d = Ohnesorge number, $\mu_f/(\rho_j d\sigma)^{1/2}$
$\bar{q}$ = jet/freestream momentum flux ratio, $\rho_j V_j^2/\rho_\infty u_\infty^2$
Re_{fd} = liquid jet Reynolds number, $\rho_j V_j d/\mu_j$
Re_{gd} = freestream Reynolds number, $\rho_\infty u_\infty d/\mu_\infty$
T_b = breakup regime parameter
t = time
u = axial velocity component
$\bar{u}_{rel}$ = relative freestream velocity, $(u_\infty - u_j)/u_\infty$
V_j = jet exit velocity
v = transverse velocity component
We_{fd} = liquid Weber number, $\rho_j d V_j^2/\sigma$
We_{gd} = relative gas Weber number, $\rho_\infty d(u_\infty - u_j)^2/\sigma$
x = axial coordinate
y = transverse coordinate
θ = injection angle
μ = molecular viscosity
ρ = mass density
τ = breakup timescale
σ = liquid surface tension

Subscripts

ab = aerodynamic breakup
b = at column breakup location
f = liquid property
fb = nonaerodynamic breakup
g = gas property
j = jet exit liquid property
∞ = freestream air property

Introduction

LIQUID jet atomization in an air crossflow is a critical process in most airbreathing propulsion systems, including turbojet, ramjet, and scramjet engines.[1–3] In these devices, liquid fuel may be injected from the combustor walls at various angles and under various operating conditions. The combustion efficiency of these devices depends heavily on the fuel distribution, which is driven by the fuel jet penetration and disintegration processes. Recently, Inamura and Nagai[4] and Wu et al.[5] have shown that the fuel distribution is very sensitive to the jet operating conditions and may be controlled through various parameters. In general, the atomization processes are quite complicated, and they are nearly impossible to predict accurately with current computational techniques. Therefore, combustor designers must rely on empirical models and correlations to develop reliable prototypes and modify existing injection schemes. The construction of robust models and correlations, however, requires an extensive database covering a very wide range of operating conditions and geometrical configurations. Although many researchers have studied the subject of normal injection in both subsonic[4–10] and supersonic flows,[11–17] the phenomena associated with angled injection into subsonic crossflows have been nearly ignored. Although some angled injection work has been conducted in the supersonic regime,[15–17] these results are not directly applicable to the subsonic regime. Therefore, it is the purpose of this investigation to examine and characterize the effects of injection angle on the breakup processes of liquid jets in subsonic crossflows.

Presented as Paper 97-2966 at the AIAA/ASME/SAE/ASEE 33rd Joint Propulsion Conference, Seattle, WA, 6–9 July 1997; received 16 July 1997; revision received 1 February 1999; accepted for publication 2 February 1999.

*Research Scientist; currently Senior Principal Engineer, Kaiser Marquardt, 16555 Saticoy Street, Van Nuys, CA 91406.
†Senior Research Scientist; currently Senior Principal Engineer, Kaiser Marquardt, 16555 Saticoy Street, Van Nuys, CA 91406.
‡Research Engineer, 2372 Lakeview Drive, Suite H.
§Branch Chief; currently Director of Engineering, Kaiser Marquardt, 16555 Saticoy Street, Van Nuys, CA 91406.

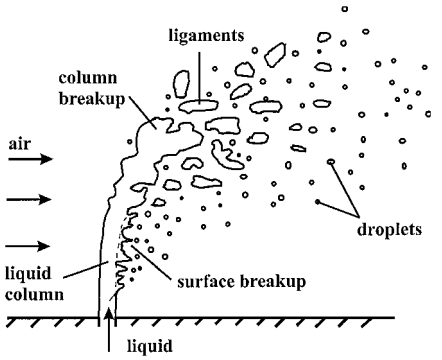

Fig. 1 Typical breakup process of a liquid jet in an air crossflow.

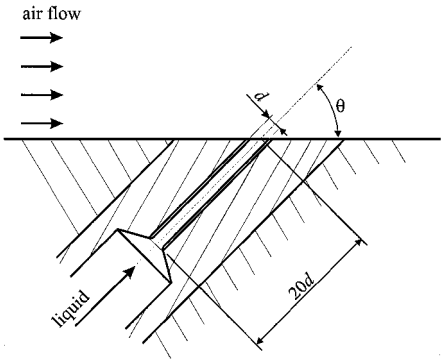

Fig. 2 Typical nozzle geometry used in present investigation.

Many previous studies of liquid injection into a crossflow of air have identified the fundamental features of jet penetration and disintegration. In general, the spray plume may be divided into three separate regions, that is, 1) the liquid column, 2) the ligament, and 3) the droplet regions (Fig. 1). The formation of the droplet region depends heavily on the ligament region, which in turn depends heavily on the liquid column breakup behavior. Therefore, a thorough understanding of the entire process must begin with complete characterization of the liquid column. The liquid column is the core of jet liquid that forms a continuous stream between the jet exit and the first point of complete fracture. This core may be turbulent or nonturbulent at the nozzle exit and will in either case exhibit distinct surface breakup characteristics.[18] Furthermore, over a wide range of jet operating conditions, liquid properties, and geometrical configurations, the liquid column appearance, length, and steadiness will vary significantly.

The objective of this study is to investigate the effects of injection angle on the near-field atomization process of liquid jets in a subsonic crossflow of air. Particular emphasis is placed on the liquid column as a first step in gaining an understanding of the complete process. Attention is focused on the column waves, trajectory, and point of fracture, and how each affects the ligament and near-field droplet regions. This paper presents 1) an account of the experimental methods; 2) qualitative descriptions of the column wave, trajectory, and surface breakup characteristics; 3) a behavioral regime map; 4) a phenomenological analysis; and 5) correlation of and comparison with experimental data.

Experimental Methods

Apparatus and Instrumentation

Liquid jets were injected into a subsonic/transonic liquid spray tunnel with the injector nozzle exit mounted flush in the bottom wall of the test section. Detailed descriptions of the design and operation of facility as well as documented flow conditions have been presented in previous studies.[19,20] The facility had a rectangular test section measuring 125 mm wide, 75 mm high, and 406 mm long. The test section had quartz windows in both side walls as well as the top wall for laser diagnostics and flow visualization. The main airflow was supplied by a series of turbine and reciprocating compressors capable of providing air mass flow rates of up to 15 kg/s with a stagnation pressure and temperature of up to 5.1 MPa and 920 K, respectively. A large exhaust system lowered and maintained the back pressure with a lower limit of nearly 20 kPa. The air Mach number in the test section was controlled by adjusting a variable-area nozzle under a choked condition downstream of the test section; the Mach number was governed by the ratio of the test section area to the nozzle throat area. This flow path generated wall boundary layers, which were typically less than 4 mm thick.

The liquid injection system consisted of a large holding tank, compressed nitrogen bottle, pressure regulator, throttling valve, coriolis-type mass flow meter, and an injector nozzle unit. The holding tank had an internal volume of approximately 0.14 m^3 and a pressure rating of 3 MPa. Prior to the experiment, the tank was filled with the test liquid, sealed, and pressurized with compressed nitrogen. The liquid mass flow rate was then controlled by adjusting the tank pressure and set according to a readout on the mass flow meter. The mass flow meter was accurate to within ±0.5% of a given reading. The measured mass flow rate was then used to determine the magnitude of the mass-averaged injection velocity at the injector exit according to $V_j = \dot{m}_j/(\rho_j A_j)$.

A typical nozzle geometry is shown in Fig. 2. Each nozzle passage had an inlet diameter of 7.62 mm followed by a 60-deg taper to a straight passage with a diameter equal to an exit diameter of 0.51 mm. In each case, the straight passage just before the jet exit had a length-to-diameter ratio of 20. These relatively large l/d resulted in liquid jets that were turbulent at the injector exit over the range of conditions tested. Finally, the transition from the tapered section to the straight passage was rounded to avoid flow cavitation.

The liquid jets issuing into the subsonic airflow were visualized using a spark-shadowgraph technique with a xenon arc lamp and nanopulser. This system provided a high-intensity light source with a pulse duration of approximately 20 ns, which could effectively freeze the motion of the liquid column and droplets. The light was collimated, passed through the test section, refocused, and then magnified. The magnification factor was set at 2.58 by choosing the appropriate optical components and path lengths. The resulting images were recorded on Polaroid Type-57 (ASA3000) black-and-white film using a 4 × 5 Speed Graphic camera with an open shutter in a darkened room. The field of view was approximately 44 × 34 mm, which provided good spatial resolution of the liquid column and near-field spray. For the test condition, four images were recorded. Each image was then digitally scanned with a spatial resolution of 150 dots per inch and was stored on magnetic disk for subsequent processing.

Test Conditions

The liquid density was measured using a hydrometer that was accurate to within 0.5 kg/m^3. A Cannon–Fenske viscometer was used to measure the liquid viscosity with a measurement uncertainty of less than 0.2%. The liquid surface tension was measured using a ring tensiometer that was accurate to within 0.0005 N/m. For the water tested, these measurements yielded a liquid density ρ_f of 997 kg/m^3, a liquid viscosity μ_f of 8.65×10^{-4} kg/m/s, and a liquid surface tension σ of 70.5×10^{-3} N/m.

Injection angles of, nominally, 30, 45, 60, 75, and 90 deg were tested. The magnitude of the liquid injection velocity was varied from 19.3 to 54.1 m/s. Tests were conducted with freestream Mach numbers of 0.2, 0.3, and 0.4, so that with the average ambient temperature of 298 K, the freestream velocities were 69.2, 103.8, and 138.4 m/s, respectively. The freestream static pressure was maintained at 140 kPa. The resulting matrix of dimensionless parameters was as follows: $12.0 \le \bar{q} \le 377$; $5.5 \le We_{gd} \le 223$; $2500 \le We_{fd} \le 19{,}600$; $3140 \le Re_{gd} \le 6280$; $10{,}900 \le Re_{fd} \le 30{,}600$; and $Oh_d = 0.00482$.

Results and Discussion

Column Wave Behavior

Flow Visualization

Figures 3 and 4 show the typical effects of injection angle on the liquid jet breakup processes for $\bar{q} = 48$ and $M_\infty = 0.2$ and 0.4, respectively. In each case, as the injection angle was decreased from 90 to 30 deg, the relative freestream velocity $\bar{u}_{\text{rel}}$ also decreased.

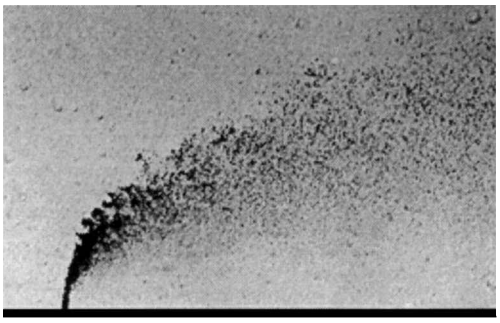

a) $\theta = 90$ deg

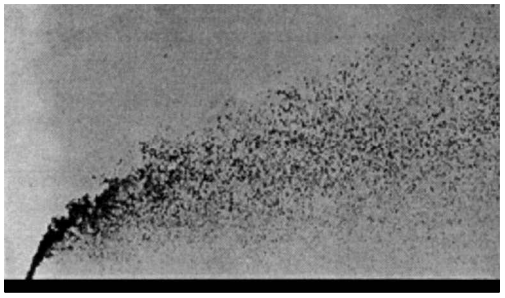

b) $\theta = 75$ deg

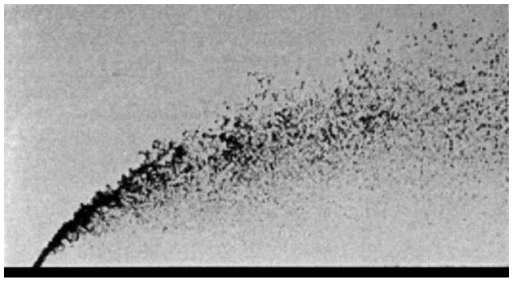

c) $\theta = 60$ deg

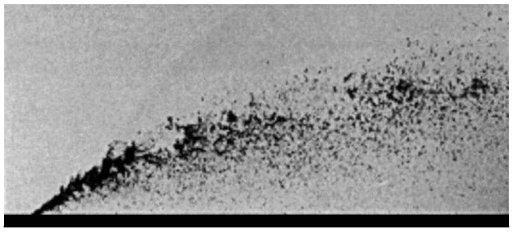

d) $\theta = 45$ deg

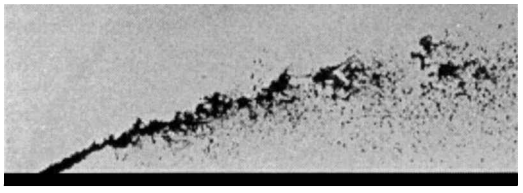

e) $\theta = 30$ deg

Fig. 3 Effects of injection angle on water jets in a subsonic crossflow: $\bar{q} = 48.1$, $M_\infty = 0.2$.

Therefore, a decrease in θ with a constant $\bar{q}$ results in a reduction of the aerodynamic forces acting on the column. When the injection angle is very shallow, the entire liquid column becomes nearly aligned with the freestream, and the flow conditions approach the case of a parallel jet in a moving stream. Furthermore, when the angle is low and the jet velocity approaches that of the freestream, the effects of liquid inertial forces and liquid turbulence on the column breakup behavior may become more apparent. The following describes how these variations in operating conditions affected the column wave behavior and jet breakup processes.

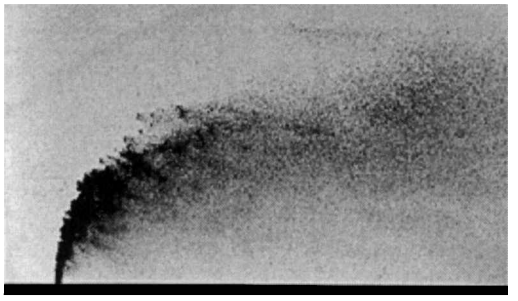

$\theta = 90$ deg

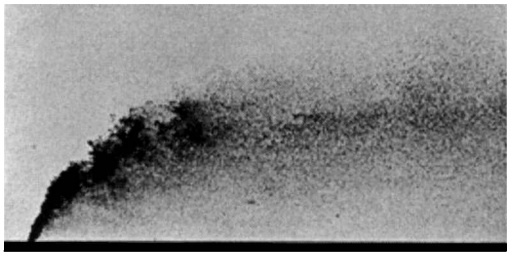

$\theta = 75$ deg

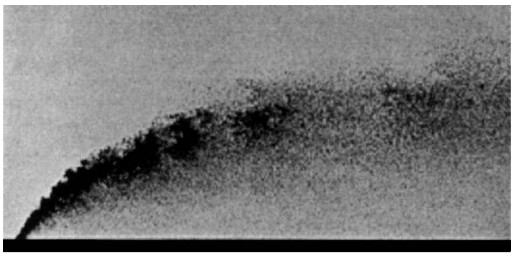

$\theta = 60$ deg

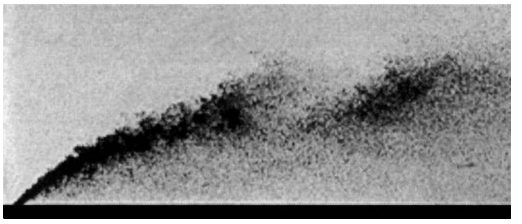

$\theta = 45$ deg

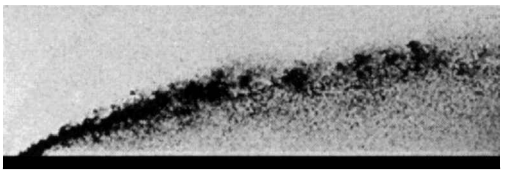

$\theta = 30$ deg

Fig. 4 Effect of injection angle on water jets in a subsonic crossflow: $\bar{q} = 48.1$, $M_\infty = 0.4$.

For the case of $M_\infty = 0.2$, shown in Fig. 3, as the injection angle was decreased, the liquid column straightened, the overall penetration decreased within the field of view, the atomization process was inhibited, and the spray appeared to become less uniform. As θ was decreased from 90 to 30 deg, $\bar{u}_{\text{rel}}$ decreased from 1.0 to 0.8, respectively. Here, u_∞ was relatively small for each of the injection angles tested and the effects of liquid turbulence on the column breakup behavior became more pronounced as the injection angle was decreased. In the 90-deg case, shown in Fig. 3a, the column fracture was preceded by the development of windward waves, and the liquid column showed no large kinks or twists prior to breakup. Schetz et al.[12] have shown that these windward waves develop as a result of aerodynamic acceleration along the direction of the column. Inamura and Nagai[4] showed that these waves are primarily

two-dimensional at low air velocities and become more complex at higher air velocities. Furthermore, they found that the disturbance wave is amplified rapidly downstream along the jet surface and results in the liquid jet disintegration. In the 30-deg case, however, shown in Fig. 3e, the liquid column, in addition to windward waves, exhibited large kinks and twists prior to complete fracture. This behavior is similar to that identified by Haenlein[21] as the sinuous wave-type breakup for liquid jets issuing into a quiescent gas medium. Examples of the sinuous wave-type breakup have been shown by Hoyt and Taylor[22] and Wu and Faeth.[23] In such cases, the jet breakup is driven by liquid turbulence, inertial forces, and liquid–air interface instabilities. Here, where u_∞ was very low, it is reasonable to expect the effects of liquid turbulence and liquid inertial force to become more pronounced. Furthermore, this transition in breakup mechanisms appeared to be accompanied by a growing periodicity in column fracture. This periodicity is evidenced by the discrete clumps of liquid that appear along the spray trajectory. These discrete clumps are produced by periodic and violent fractures of the liquid column similar to that described by Sherman and Schetz,[11] where the breakup mechanism was characterized by gross jet fracture, as opposed to surface disintegration. For liquid jets in a coaxial air flow, Chigier and Reitz[24] classified this type of behavior as a pulsating breakup submode, where different jet instabilities, such as capillary helical, and Kelvin–Helmholtz instabilities, dominate the mechanisms. It was stated that this behavior occurs in all sprays to some lesser or greater extent. Finally, atomization was inhibited with decreasing angle, as is clearly indicated by the relative average drop size at the end of the field of view.

The case of $M_\infty = 0.4$, shown in Fig. 4, exhibited behavior similar to the preceding case, that is, as the injection angle decreased, the liquid column became straighter, the overall penetration decreased within the field of view, and the atomization process was inhibited and became more unsteady. As θ was decreased from 90 to 30 deg, $\bar{u}_{\text{rel}}$ again decreased from 1.0 to 0.8. In this case, however, u_∞ was much higher than in the earlier case, and the enhanced effects of the aerodynamic forces became quite apparent. The increased aerodynamic forces greatly augmented the atomization process, and the characteristics of nonaerodynamic column breakup (those resulting from liquid turbulence and liquid inertial forces) could not be identified. At low injection angles, however, and especially for $\theta = 30$ deg, the jet structure takes on an appearance very similar to a coaxial jet with significant aerodynamic forces. For a liquid jet in a coaxial air flow, Chigier and Reitz[24] have classified this type of breakup as the fiber-type breakup mode, where the atomization begins with the formation of fibers and their peeling off the main liquid core. Furthermore, the increase in crossflow air velocity caused the pulsating nature of the spray to become more pronounced. This behavior was also observed by Chigier and Reitz[24] for coaxial jets and was classified as a superpulsating disintegration submode. It was determined that, for coaxial jets, this type of disintegration occurs when a low liquid mass flow rate is conjoined with a very high gas velocity.

A comparison of Figs. 3 and 4 for equal injection angles, with $\bar{q}$ being held constant, shows that there was no apparent change in the overall penetration with the increase in u_∞. Thus, for a given θ, the jet-to-freestream dynamic pressure ratio $\bar{q}$ remains the dominant factor in determining jet penetration, even when the θ is small.

Figures 5 and 6 show the effects of $\bar{q}$ on angled liquid jets in a $M_\infty = 0.3$ crossflow with $\theta = 60$ and 30 deg, respectively. In each case, $\bar{q}$ was varied from 21 to 168, which resulted in a moderate reduction of $\bar{u}_{\text{rel}}$. For $\theta < 90$ deg, it is not possible to change $\bar{q}$ without varying $\bar{u}_{\text{rel}}$. The preceding observations suggest, however, that variations in u_∞ for a given θ and $\bar{q}$ do not affect jet penetration. Therefore, the variations in jet penetration for a constant θ and d may be attributed to $\bar{q}$ alone, although the breakup mechanisms may not.

For the case of $\theta = 60$ deg, shown in Fig. 5, the penetration increased, the trajectory became straighter, and the liquid column increased in length as $\bar{q}$ was increased. As $\bar{q}$ increased from 21 to 168, $\bar{u}_{\text{rel}}$ decreased from 0.93 to 0.81, respectively. Although this is only a moderate change in $\bar{u}_{\text{rel}}$, its potential effect on the breakup mechanisms must be noted. At each $\bar{q}$, the breakup process appeared to be fairly uniform, as no large clumps of liquid were observed in the spray. As $\bar{q}$ increased, however, the liquid column became straighter, thinner, and more distinct. Furthermore, column wave development

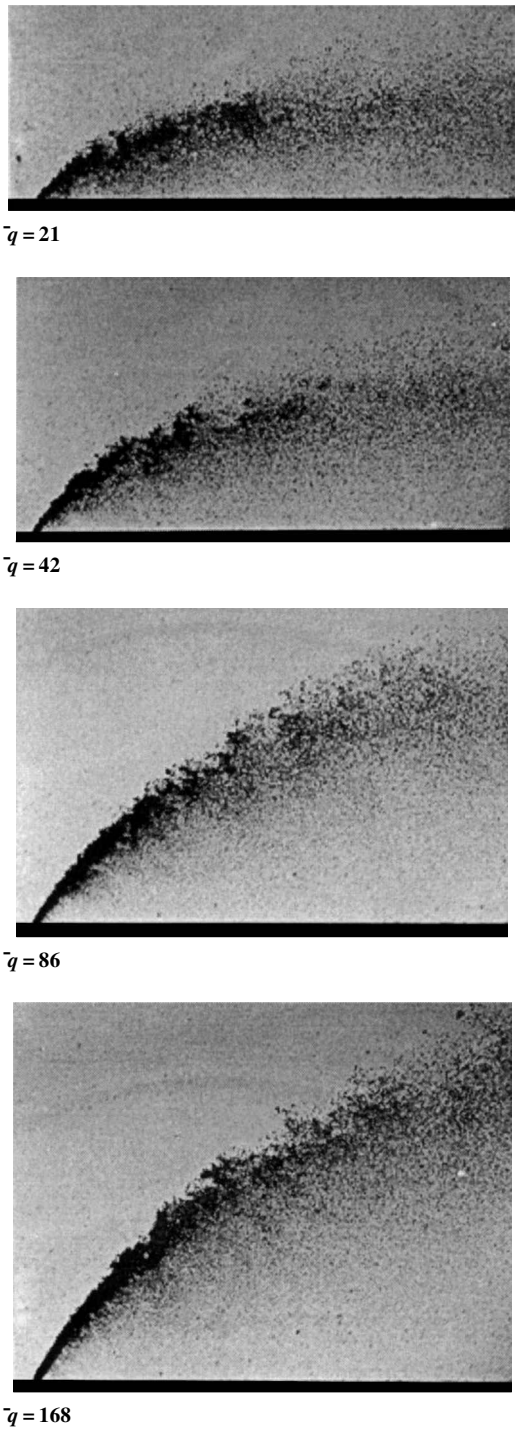

Fig. 5 Effect of $\bar{q}$ on angled water jets in a subsonic crossflow: $\theta = 60$ deg, $M_\infty = 0.3$.

appeared to be suppressed as the liquid column lengthened with increasing $\bar{q}$. Finally, at higher $\bar{q}$, thin threads of liquid being stripped away from the liquid column could be observed near the jet exit.

The case of $\theta = 30$ deg, shown in Fig. 6, exhibited behavior similar to the earlier case. That is, as $\bar{q}$ was increased, the penetration increased, the trajectory became straighter, and the liquid column increased in length. As $\bar{q}$ was increased from 21 to 168, $\bar{u}_{\text{rel}}$ decreased from 0.89 to 0.68, respectively. Again, although this is only a moderate change in $\bar{u}_{\text{rel}}$, its potential effect on the breakup mechanisms must be noted. Unlike the preceding case, however, the effects of liquid turbulence on the column could be observed, and the behavior appeared more periodic at the lower $\bar{q}$. At the lower $\bar{q}$, the liquid column developed large waves, and it became quite distorted and kinked prior to complete fracture, with an appearance similar to fiber-type breakup mode identified by Chigier and Reitz.[24] The

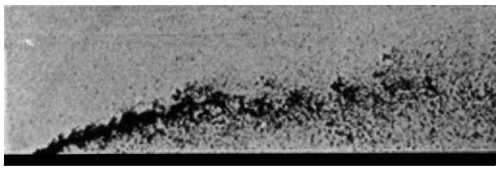

$\bar{q} = 21$

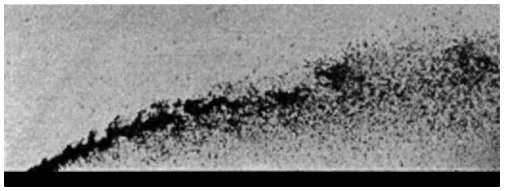

$\bar{q} = 42$

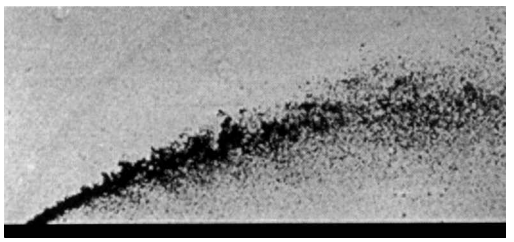

$\bar{q} = 86$

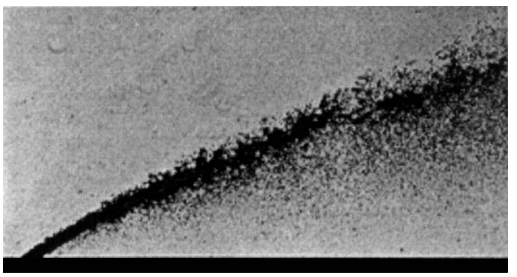

$\bar{q} = 168$

Fig. 6 Effect of $\bar{q}$ on angled water jets in a subsonic crossflow: $\theta = 30$ deg, $M_\infty = 0.3$.

overall trajectory of the liquid column, however, appeared to be relatively straight. This was expected because the aerodynamic drag force is nearly aligned with the liquid column and should not result in much curvature. Therefore, it is reasonable to suspect that fluidic mechanisms within the jet, rather than aerodynamic mechanisms acting on the jet, may be more significant and possibly dominate the column breakup process. At the higher $\bar{q}$, unlike the lower $\bar{q}$, the column exhibited small surface waves and showed little distortion in the form of kinks or twists. Again, the column showed very little curvature in the freestream direction, indicating a minor influence of aerodynamic forces on the column trajectory prior to fracture.

Breakup Regimes

The preceding observations indicate that the column breakup process may be divided into two distinct regimes: aerodynamic and nonaerodynamic. For aerodynamic breakup, the aerodynamic forces associated with the gaseous crossflow accelerate the column in the freestream direction and induce unstable surface waves that ultimately lead to column fracture. For nonaerodynamic breakup, liquid turbulence and liquid inertial forces generate instabilities within the liquid itself and cause large-scale column deformations, which ultimately lead to column fracture. The dominance of either regime is governed by the jet operating conditions, although, both mechanisms are present to some extent in both cases. As was observed earlier, $\bar{u}_{\text{rel}}$, u_∞, and $\bar{q}$ played an important role in the appearance of these different characteristics. To predict breakup behavior based on operating conditions, a breakup regime parameter T_b, to be presented subsequently, was defined as the ratio of the aerodynamic breakup timescale to the nonaerodynamic breakup timescale. Using this definition, $T_b < 1$ indicates a dominance of aerodynamic forces, whereas $T_b > 1$ indicates a dominance of liquid forces. Figure 7 shows a map of θ vs T_b and the corresponding breakup regimes over the entire range of test conditions. Visual scrutiny of the entire set of images revealed that, indeed, a line dividing the appearance of aerodynamic and nonaerodynamic breakup characteristics could be drawn at approximately $T_b \approx 1$. Near $T_b = 1$, however, the predominant breakup mechanism was not always obvious, and the mixed-type of behavior was classified as residing in a transition region. This transition region was very narrow as it did not extend beyond $0.9 < T_b < 1.5$. Although the visual distinction between breakup characteristics is rather subjective at this point, the threshold will be substantiated in quantifiable terms to be discussed later. The location of column fracture and, therefore, the column length is governed by the prevalent breakup regime. Therefore, as will be shown, the appropriate timescale for the column breakup length will be decisive in determining the corresponding breakup regime.

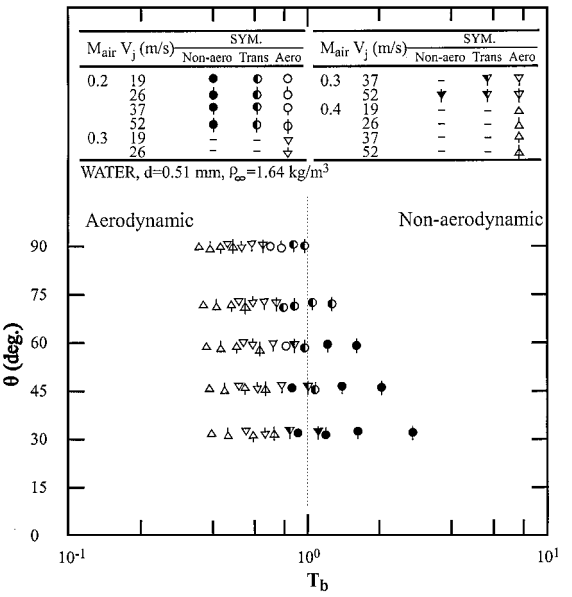

Fig. 7 Regime map of column breakup behavior.

Column Trajectory and Fracture

Liquid Column Trajectory

Previous investigations have focused primarily on the measurement of overall spray trajectories where small droplets dominate the mixing process in the far-field regions. As a result, the liquid column trajectory predictions are not optimized within their respective regime. That is, the overall trajectory prediction may not fit the column trajectory as well as a correlation developed for that regime alone. In a study conducted by Wu et al.,[10] however, the liquid column trajectories were analyzed by balancing the liquid acceleration with the aerodynamic drag forces in the airstream direction. This phenomenological analysis provided simple correlations based on fundamental physics without the need for numerical solutions of complicated governing equations. Furthermore, such a model of the liquid column regime provides a first step in modeling the entire atomization process. The same approach was used in the present investigation.

In this study, the trajectory of the liquid column was modeled by considering a cylindrical element of fluid subject to an aerodynamic drag force. This situation is shown in the force diagram in Fig. 8. An element of fluid emerging from the jet exit is assumed to have a constant diameter equal to the jet exit diameter d and length l, as it moves along the column trajectory. These assumptions neglect column deformation, evaporation, and droplet dispersion, though these effects will be accounted for later by introducing an average drag coefficient. As the fluid element exits the jet orifice, it has an initial velocity V_j at an initial angle equal to the injector angle θ. The air crossflow will cause the element to undergo a change in momentum as it accelerates in the direction of the aerodynamic drag

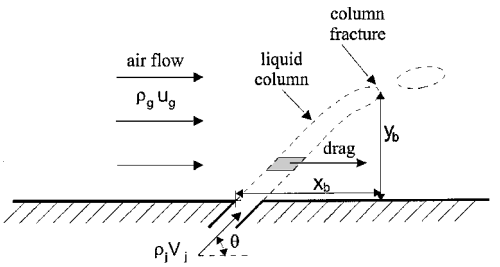

Fig. 8 Force diagram used in the present analysis.

force. The drag force is assumed to be parallel to the freestream direction over the entire length of the column, and the effects of gravity are neglected. As a result, the fluid element will be deflected into the direction of the freestream. By introducing an average drag coefficient C_D, the axial momentum equation can be written as follows:

$$\frac{\pi}{4}\rho_f d^2 l\frac{\mathrm{d}u_f}{\mathrm{d}t} = \frac{1}{2}C_D\rho_g(u_g-u_f)\left[(u_g-u_f)^2+(v_g-v_f)^2\right]^{\frac{1}{2}} ld \quad (1)$$

To render Eq. (1) more tractable, the following considerations were made. For the present investigation, $(v_g - v_f)^2$ was estimated to be considerably less than $(u_g - u_f)^2$ in most cases and was therefore neglected. Additionally, the variation in u_f was, in most cases, very small as compared to u_g, so that the approximation $u_g - u_f \approx u_g - u_j$ could be made. Finally, ρ_g and u_g were assumed to remain constant at their respective freestream values, and ρ_f and u_f were assumed to remain constant at their respective jet exit values, ρ_j and u_j. The following summarizes these assumptions used in the subsequent derivation:

$$(v_g - v_f)^2 \ll (u_g - u_f)^2, \qquad u_g - u_f \approx u_g - u_j$$

$$\rho_g = \rho_\infty = \text{const}, \qquad \rho_f = \rho_j = \text{const}$$

$$u_g = u_\infty = \text{const}, \qquad v_f = v_j = V_j \sin\theta = \text{const}$$

Using these assumptions, the axial momentum equation (1) was reduced to

$$\frac{\mathrm{d}u_f}{\mathrm{d}t} = \frac{2C_D}{d\pi}\frac{\rho_\infty}{\rho_j}(u_\infty - u_j)^2 \quad (2)$$

so that integration of the axial momentum equation with respect to time yielded

$$u_f = \frac{2C_D}{d\pi}\frac{\rho_\infty}{\rho_j}(u_\infty - u_j)^2 t + u_j \quad (3)$$

With $u_f = \mathrm{d}x/\mathrm{d}t$, a second integration with respect to time yielded

$$x = \frac{C_D}{d\pi}\frac{\rho_\infty}{\rho_j}(u_\infty - u_j)^2 t^2 + u_j t \quad (4)$$

Because the transverse velocity of the liquid column was assumed to be constant and equal to the transverse component of the jet exit velocity, $v_f = \mathrm{d}y/\mathrm{d}t = v_j$, then $y = v_j t$, and the trajectory equation could be written as

$$\frac{x}{d} = \frac{C_D}{\pi}\frac{\rho_\infty}{\rho_j}\frac{(u_\infty - u_j)^2}{v_j^2}\left(\frac{y}{d}\right)^2 + \frac{u_j}{v_j}\left(\frac{y}{d}\right) \quad (5)$$

Equation (5) could then be expressed in terms of the jet-to-freestream momentum flux ratio $\bar{q}$ and the injection angle θ as follows:

$$\frac{x}{d} = \frac{1}{\pi}\frac{C_D}{\bar{q}\sin^2\theta}\left(1 - \frac{V_j\cos\theta}{u_\infty}\right)^2\left(\frac{y}{d}\right)^2 + \frac{\cos\theta}{\sin\theta}\left(\frac{y}{d}\right) \quad (6)$$

The actual liquid column trajectories were obtained from digitally scanned images of the shadowgraphs. The data acquisition procedure was automated by using in-house image processing software developed specifically for spray analysis. With the image displayed on the computer screen, the user was prompted to indicate, using the mouse pointer, the point of jet exit and the point of column fracture near the windward surface. The user was then prompted to identify 18 points, equally spaced in the vertical dimension, on the windward column surface between the jet exit and point of fracture. These coordinates were then stored in a file for subsequent analysis. This procedure was performed on each of the four images produced for each of the 60 different test conditions yielding a total of nearly 5000 test points. Using these results, an average drag coefficient was iteratively determined such that the final value for C_D yielded an average ratio of predicted-to-measured values equal to one.

The resulting overall average of C_D was 4.39 with an overall standard deviation of less than 30%. A higher drag coefficient is required for cases where θ was very low and $\bar{q}$ was very high. In those cases, the original assumptions in the derivation of the trajectory equation begin to break down, and applicability approaches a limit. When θ is very low and $\bar{q}$ is very high, however, the trajectory is dominated by the linear term of Eq. (6), and the effect of C_D becomes much less significant. Thus, the lower, averaged C_D provides a good prediction of the column trajectory over the entire range of operating conditions tested.

The average drag coefficient of $C_D = 4.39$ determined in the present investigation is significantly higher than the value of 1.70 previously determined by Wu et al.[10] It is suspected that significant facility modifications, which resulted in a thinner boundary layer (by a factor of 2), may have caused the discrepancy in results. Furthermore, differences in injector nozzle design and passage lengths may also have contributed to the disparity. Both values of C_D, however, are larger than the drag coefficients for flow passing over a solid circular cylinder[25] and for the theoretical predictions of liquid injection by Adelberg[26] and Nguyen and Karagozian.[27] The larger values may be due to significant column deformation not accounted for in the model.

The predicted column trajectories for $x/d > 1$ were plotted against the measured column trajectories as shown in Fig. 9. The average ratio of predicted-to-measured x/d values was 1.000 with a standard deviation of less than 15%. For longer column lengths, the correlation tended to overpredict the column penetration. This is a result of the use of an average drag coefficient that was biased by the abundance of shorter column lengths, which generally had lower drag coefficients. Furthermore, the cases where the column lengths were very long were those where θ was very low and $\bar{q}$ was very high. Again, these cases stretch the applicability of the original assumptions to their limit and result in an exaggeration of the predicted linearity of the column trajectory. The underprediction of the x/d are within one standard deviation σ for most cases.

Fracture Location

The column fracture location was modeled using the timescale for the aerodynamic secondary breakup of a spherical droplet and the breakup timescale for a turbulent liquid jet issuing into a quiescent

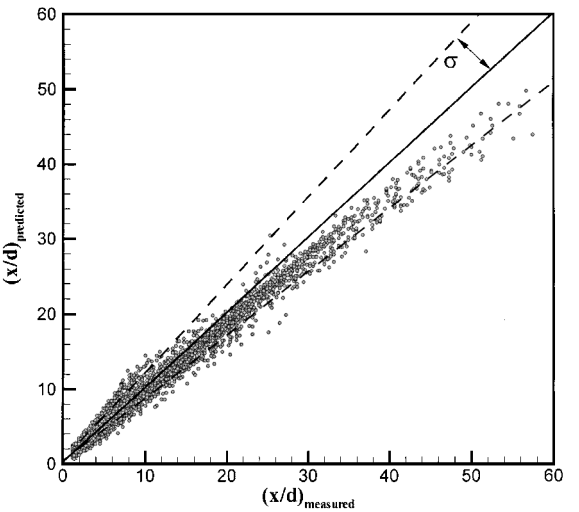

Fig. 9 Predicted vs measured column trajectories.

gas. The former approach was first applied by Wu et al.[10] and was deemed plausible because the breakup mechanisms for columns and droplets, subject to significant aerodynamic forces, are very similar. Furthermore, Hsiang and Faeth[28] indicated that the timescale for shear breakup determined by Ranger and Nicholls[29] was also applicable to other breakup regimes. The aerodynamic breakup timescale τ_{ab} for a liquid jet with an initial streamwise velocity u_j could be written as

$$\tau_{ab} = C_{ab}\frac{d}{u_\infty - u_j}\sqrt{\frac{\rho_j}{\rho_\infty}} \tag{7}$$

In cases where $(u_\infty - u_j)$ was small, however, the effects of nonaerodynamic breakup mechanisms caused the column to fracture with a length much shorter than that predicted by the aerodynamic timescale. In these cases, a timescale for breakup of a turbulent liquid jet issuing into a quiescent medium was employed. This timescale was obtained by assuming that the column length is proportional to cubic root of the liquid Weber number. This was justified by the results of Grant and Middleman,[30] Chen and Davis,[31] and Wu and Faeth.[23] Then, assuming that the liquid velocity remains constant along the entire liquid core [neglecting acceleration in the freestream direction due to aerodynamic forces is justified because $(u_\infty - u_j)$ was very small in these cases] the timescale for breakup of a turbulent jet resulting from nonaerodynamic mechanisms may be written as

$$\tau_{fb} = C_{fb}(d/V_j)We_{fd}^{\frac{1}{3}} \tag{8}$$

With the appropriate constants of proportionality, C_{ab} and C_{fb}, the shorter timescale will ultimately determine the point of fracture. This criterion may be established by combining Eqs. (7) and (8) to form the following parameter:

$$T_b = \frac{\tau_{ab}}{\tau_{fb}} = \frac{C_{ab}}{C_{fb}}\frac{V_j}{u_\infty - u_j}\sqrt{\frac{\rho_j}{\rho_\infty}}We_{fd}^{-\frac{1}{3}} \tag{9}$$

The constants C_{ab} and C_{fb} can be empirically determined from the measured column lengths. It is important to note that whereas C_{ab} and C_{fb} may vary with gas and liquid properties and may show facility dependence, the crossover between aerodynamic and nonaerodynamic breakup will, by definition, always occur at T_b equal to unity.

The preceding timescales for the completion of the column breakup were used to determine the distance required for the liquid column to fracture under the given conditions. Because the transverse component of the injectant velocity is assumed to remain constant up to the point of fracture, the transverse breakup distance may then be obtained using

$$\frac{y_b}{d} = C_{ab}\frac{V_j\sin\theta}{u_\infty - V_j\cos\theta}\sqrt{\frac{\rho_j}{\rho_\infty}} = C_{ab}\frac{L_{ab}}{d} \tag{10}$$

for aerodynamic breakup ($T_b < 1$), or

$$y_b/d = C_{fb}We_{fd}^{\frac{1}{3}}\sin\theta = C_{fb}(L_{fb}/d) \tag{11}$$

for nonaerodynamic breakup ($T_b > 1$), where L_{ab} and L_{fb} are the aerodynamic and nonaerodynamic column length scales, respectively. The axial fracture distance x_b/d was then determined by substituting either Eq. (10) or Eq. (11), whichever was appropriate, into Eq. (6). This resulted in the following relations:

$$\frac{x_b}{d} = \frac{C_D C_{ab}^2}{\pi} + C_{ab}\frac{V_j\cos\theta}{u_\infty - V_j\cos\theta}\sqrt{\frac{\rho_j}{\rho_\infty}} \tag{12}$$

for aerodynamic breakup ($T_b < 1$), or

$$\frac{x_b}{d} = \frac{1}{T_b^2}\frac{C_D C_{ab}^2}{\pi} + C_{fb}We_{fd}^{\frac{1}{3}}\cos\theta \tag{13}$$

for nonaerodynamic breakup ($T_b > 1$). Note that when $\theta = 90$ deg, x_b/d will be a constant for $T_b < 1$ and will vary inversely with T_b^2 for $T_b > 1$.

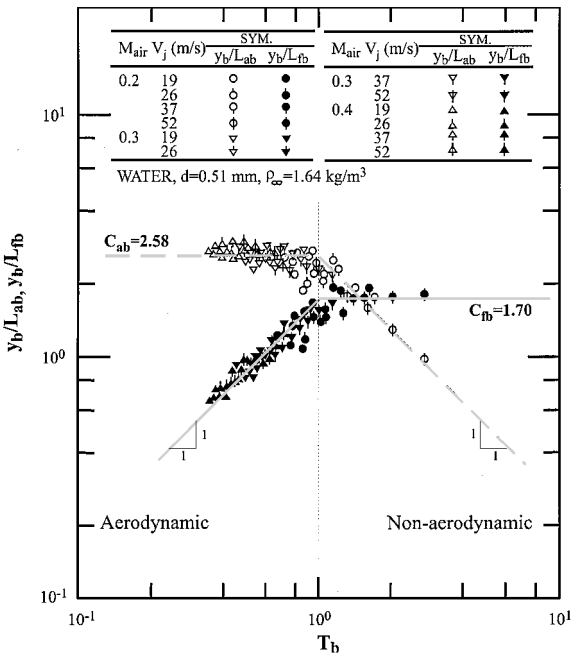

Fig. 10 Liquid column length scales.

The breakup coefficients C_{ab} and C_{fb} were determined by plotting y_b/L_{ab} and y_b/L_{fb} for each condition over the entire range of T_b. By the examination of Fig. 10, the value and range of applicability for each coefficient could be determined and observed, respectively. For $T_b < 1$, the ratio y_b/L_{ab} was relatively constant, although, $T_b > 1$, the ratio y_b/L_{ab} was proportional to T_b^{-1}. Likewise, for $T_b > 1$, the ratio y_b/L_{fb} was relatively constant, whereas for $T_b < 1$, the ratio y_b/L_{fb} was proportional to T_b. Because T_b is equal to the ratio τ_{ab}/τ_{fb} and, therefore, L_{ab}/L_{fb}, coordinate y_b should scale with L_{ab} for $T_b < 1$ and L_{fb} for $T_b > 1$. The average C_{ab} for $T_b < 1$ was 2.58 with a standard deviation of less than 23%; Wu et al.[10] obtained a constant of 3.44. The average C_{fb} for $T_b > 1$ was 1.70, with a standard deviation of less than 17%. The constant of proportionality for T_b in Eq. (9) was then determined to be $C_{ab}/C_{fb} = 1.52$. Hence, Eq. (9) could be used to determine the breakup regime and, therefore, the appropriate correlations for the breakup coordinates based on whether T_b is less than or greater than unity.

It should be noted that for $T_b < 1$ and $\theta = 90$ deg, Eq. (12) yields a constant of $x_b/d = 9.30$. Wu et al.[10] obtained a predicted value of 6.40. Again, as in the case of the drag coefficient, the difference may be attributed to a thinner boundary layer. With the thinner boundary layer, the average C_D will be larger and C_{ab} will be smaller. In this case, C_D was much more sensitive to the change in boundary-layer thickness, so that the breakup distance increased. These results, however, may differ for varying fluid properties.

Figure 11 shows the predicted vs measured column fracture heights. The overall prediction was quite good with an average ratio of predicted-to-measured values of 1.00 and a standard deviation of 10.3%. The scatter appears to be large for large y/d, although the percent differences are comparable to data at the smaller y/d.

Figure 12 shows the results of the predicted vs measured column fracture distances. In this case, the average ratio of predicted-to-measured values was 0.95, with a standard deviation of 13.9%. Again, the scatter appears to be large for large x/d, although, the percent differences are comparable to data at the smaller x/d. Note that for $T_b < 1$ and $\theta = 90$ deg, the breakup distance was fairly constant with an average value of 9.10, which was within 2.2% of the predicted value of 9.30.

Summary of Empirical Correlations

The following is a summary of the analytical/empirical relations obtained in this investigation. Although the constants may only reflect those case tested here, the trends should apply to other cases as well.

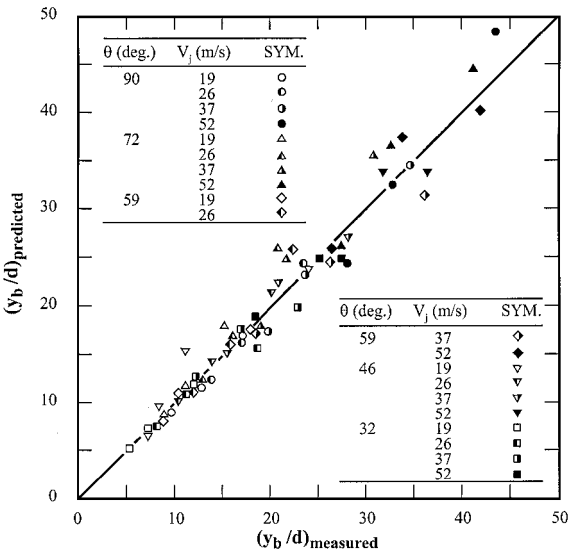

Fig. 11 Predicted vs measured column fracture height.

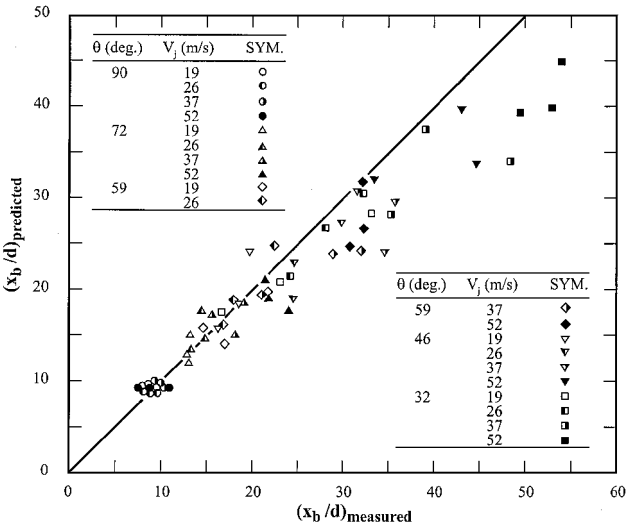

Fig. 12 Predicted vs measured column fracture distance.

Column trajectory:

$$\frac{x}{d} = \frac{1}{\pi}\frac{4.4}{\bar{q}\sin^2\theta}\left(1 - \frac{V_j\cos\theta}{u_\infty}\right)^2\left(\frac{y}{d}\right)^2 + \frac{\cos\theta}{\sin\theta}\left(\frac{y}{d}\right) \qquad (14)$$

Breakup regime parameter:

$$T_b = \frac{3}{2}\frac{V_j}{u_\infty - V_j\cos\theta}\sqrt{\frac{\rho_j}{\rho_\infty}}We_{fd}^{-\frac{1}{3}} \qquad (15)$$

Column fracture height:

$$\frac{y_b}{d} = 2.6\frac{V_j\sin\theta}{u_\infty - V_j\cos\theta}\sqrt{\frac{\rho_j}{\rho_\infty}}, \qquad T_b < 1 \qquad (16)$$

$$\frac{y_b}{d} = 1.7We_{fd}^{\frac{1}{3}}\sin\theta, \qquad T_b > 1 \qquad (17)$$

Column fracture distance:

$$\frac{x_b}{d} = 9.3 + 2.6\frac{V_j\cos\theta}{u_\infty - V_j\cos\theta}\sqrt{\frac{\rho_j}{\rho_\infty}}, \qquad T_b < 1 \qquad (18)$$

$$\frac{x_b}{d} = \frac{9.3}{T_b^2} + 1.7We_{fd}^{\frac{1}{3}}\cos\theta, \qquad T_b > 1 \qquad (19)$$

The preceding empirical correlations can thus be used to predict, with a good degree of accuracy, the column trajectory, column length, and spray appearance, for angled water jets in a subsonic crossflow of air operating within the limits of conditions tested in this investigation. As a check, a computer program was written to superimpose predicted trajectories and breakup locations on arbitrarily chosen spray images. Figure 13 shows two typical spray images with predicted trajectory overlays; the circles indicate the predicted fracture location. For nearly all cases, the qualitative comparisons were comparable to those presented in Fig. 13. Cases that did not compare as well were those where θ was very low and V_j was very high. In those cases, the column linearity was overpredicted, which resulted in a slight overprediction of the penetration near the point of column fracture.

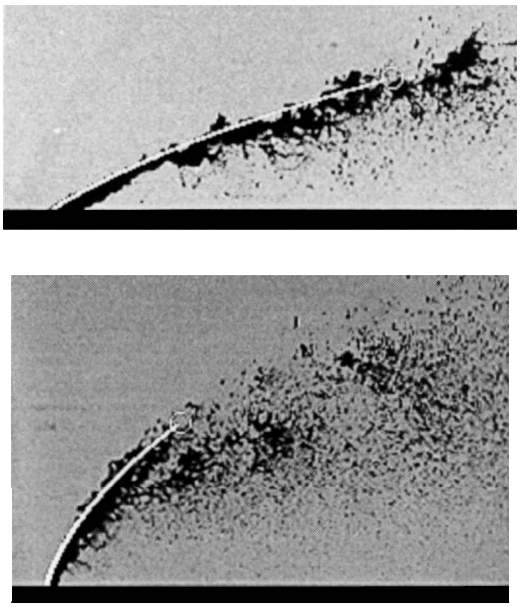

Fig. 13 Spray images with predicted column trajectory overlays.

Summary and Conclusions

The effects of injection angle on the breakup processes of turbulent liquid jets in a subsonic crossflow were investigated both experimentally and analytically. With water as the test liquid, the injection angle, air Mach number, and injection velocity were varied over a wide range of operating conditions to provide a large database of experimental results. Liquid column trajectories, fracture locations, and near-field spray characteristics were ascertained through pulsed shadowgraph photography and digital image processing techniques. Data were used to substantiate empirical constants required for closure of derived analytical relations. These relations were developed to predict liquid column trajectories, breakup regime, and column fracture locations. These results form a foundation from which the development of a complete spray model may be constructed. The results of this investigation may be summarized as follows:

1) For a given set of operating conditions, with decreasing injection angle, the liquid column straightens, the column penetration decreases, the atomization process is inhibited, and column fracture becomes periodic in nature. Furthermore, a decrease in the injection angle causes an increase in the axial component of the jet velocity and, therefore, a decrease in the relative velocity between the liquid and the air. This causes the breakup regime parameter T_b to decrease and may cause a transition in the breakup regime.

2) Column fracture locations are correlated with jet operating conditions and depend on the corresponding breakup regime as determined by the breakup regime parameter T_b. For $T_b > 1$, the column fracture is governed by nonaerodynamic breakup, such as a turbulent liquid jet in a quiescent gas. For $T_b < 1$, the column fracture is governed by aerodynamic breakup, and the column length scales with the time for the analogous aerodynamic secondary breakup of a liquid droplet.

3) For $T_b < 1$, the column breakup is largely dominated by aerodynamic mechanisms. The liquid column exhibits well-defined,

two-dimensional windward surface waves and does not develop any large kinks or twists prior to breakup. As T_b is decreased, these surface waves become more complex, and the atomization process is enhanced. For very small T_b and $\theta < 90$ deg, the liquid column may exhibit a fiber-type breakup and may also exhibit a pulsating behavior; these effects become more pronounced as θ is decreased.

4) For $T_b > 1$, column breakup is largely dominated by nonaerodynamic mechanisms; that is, the breakup is driven by liquid turbulence and liquid inertial forces. As T_b is increased, the liquid column becomes very straight and the atomization process is inhibited. For low air velocities, the liquid column exhibits large waves, kinks, and twists prior to breakup and may also exhibit a pronounced pulsating behavior for $\theta < 90$ deg.

5) Regardless of breakup regime, the liquid column trajectory is correlated with the jet-to-freestream momentum flux ratio $\bar{q}$, injection angle θ, and an empirically determined drag coefficient C_D. The trajectory equation has a binomial form and is derived from a simple force balance and momentum analysis. The equation indicates that for low $\bar{q}$ and high θ, the squared term is dominant, and the column exhibits a large degree of curvature. For high $\bar{q}$ and low θ, however, the linear term is dominant, and the column is straighter. These predictions are in complete accordance with experimental observation.

As a final note, the results presented here are, of course, limited to water injected into an air crossflow. Future studies should investigate the effects of liquid properties and crossflow gas properties. Furthermore, the effects of boundary-layer thickness and profile shape will affect the empirically determined constants and must be considered before applying the equations presented in this study. Studies are being conducted to resolve the effects of boundary-layer shape and thickness on the empirically determined drag coefficient.

Acknowledgments

This work was sponsored by and performed at the U.S. Air Force Research Laboratory, Wright–Patterson Air Force Base, Ohio, under Contract F33615-96-C-2614. The authors would like to acknowledge the assistance provided by the Air Facilities Group of the U.S. Air Force Research Laboratory. The authors would also like to thank Anna Creese of Taitech for her editorial consultation.

References

[1]Hojnacki, J. T., "Ramjet Engine Fuel Injection Studies," U.S. Air Force Aeropropulsion Lab., AFAPL-TR-72-76, Wright–Patterson AFB, OH, 1972.

[2]Wotel, G. J., Gallagher, K. E., Caron, S. D., Rosfjord, T. J., Hautman, D. J., and Spadaccini, L. J., "High Speed Turboramjet Combustor Technology Program," U.S. Air Force Research Lab., TR-91-2043, Wright–Patterson AFB, OH, 1991.

[3]Yates, C. L., "Liquid Injection Into a Supersonic Stream," U.S. Air Force Aeropropulsion Lab., Vol. 1, AFAPL-TR-71-91, Wright–Patterson AFB, OH, 1972.

[4]Inamura, T., and Nagai, N., "Spray Characteristics of Liquid Jet Traversing Subsonic Airstreams," *Journal of Propulsion and Power*, Vol. 13, No. 2, 1997, pp. 250–256.

[5]Wu, P.-K., Kirkendall, K. A., Fuller, R. P., and Nejad, A. S., "Spray Structures of Liquid Jets Atomized in Subsonic Crossflows," *Journal of Propulsion and Power*, Vol. 14, No. 2, 1998, pp. 173–181.

[6]Schetz, J. A., and Padhye, A., "Penetration and Breakup of Liquids in Subsonic Airstreams," *AIAA Journal*, Vol. 15, No. 10, 1977, pp. 1385–1390.

[7]Ingebo, R. D., "Aerodynamic Effects of Combustor Inlet-Air Pressure on Fuel Jet Atomization," AIAA Paper 84-1320, June 1984.

[8]Wu, P.-K., Hsiang, L.-P., and Faeth, G. M., "Aerodynamic Effects of Primary and Secondary Spray Breakup," *Liquid Rocket Engine Combustion Instability*, edited by V. Yang and W. Anderson, Vol. 169, Progress in Astronautics and Aeronautics, AIAA, Washington, DC, 1995, pp. 247–279.

[9]Chen, T. H., Smith, C. R., Schommer, D. G., and Nejad, A. S., "Multi-Zone Behavior of Transverse Liquid Jet in High-Speed Flow," AIAA Paper 93-0453, Jan. 1993.

[10]Wu, P.-K., Kirkendall, K. A., Fuller, R. P., and Nejad, A. S., "Breakup Processes of Liquid Jets in Subsonic Crossflows," *Journal of Propulsion and Power*, Vol. 13, No. 1, 1997, pp. 64–73.

[11]Sherman, A., and Schetz, J. A., "Breakup of Liquid Sheets and Jets in a Supersonic Gas Stream," *AIAA Journal*, Vol. 9, No. 4, 1971, pp. 666–673.

[12]Schetz, J. A., Kush, E. A., and Joshi, P. B., "Wave Phenomena in Liquid Jet Breakup in a Supersonic Crossflow," *AIAA Journal*, Vol. 18, No. 7, 1980, pp. 774–778.

[13]Nejad, A. S., and Schetz, J. A., "Effects of Viscosity and Surface Tension on a Jet Plume in Supersonic Crossflow," *AIAA Journal*, Vol. 22, No. 4, 1984, pp. 653–659.

[14]Heister, S. D., Nguyen, T. T., and Karagozian, A. R., "Modeling of Liquid Jets Injected Transversely Into a Supersonic Crossflow," *AIAA Journal*, Vol. 27, No. 12, 1989, pp. 1727–1734.

[15]Kolpin, M. A., Horn, K. P., and Reichenbach, R. E., "Study of Penetration of a Liquid Injectant into a Supersonic Flow," *AIAA Journal*, Vol. 6, No. 5, 1968, pp. 853–858.

[16]Catton, I., Hill, D. E., and McRae, R. P., "Study of Liquid Jet Penetration in a Hypersonic Stream," *AIAA Journal*, Vol. 6, No. 11, 1968, pp. 2084–2089.

[17]Baranovsky, S. I., and Schetz, J. A., "Effect of Injection Angle on Liquid Injection in Supersonic Flow," *AIAA Journal*, Vol. 18, No. 6, 1980, pp. 625–629.

[18]Wu, P.-K., Miranda, R. F., and Faeth, G. M., "Effects of Initial Flow Conditions on Primary Breakup of Nonturbulent and Turbulent Round Liquid Jets," *Atomization and Sprays*, Vol. 5, No. 2, 1995, pp. 175–196.

[19]Chen, T. H., Roe, L. A., and Nejad, A. S., "Multifunction Droplet Imaging and Velocimetry System for Spray Jets," *Journal of Propulsion and Power*, Vol. 10, No. 6, 1994, pp. 798–803.

[20]Raffoul, C. N., Nejad, A. S., Gould, R. D., and Spring, A. S., "An Experimental and Numerical Study of the Isothermal Flowfield Behind a Bluff Body Flameholder," American Society of Mechanical Engineers, ASME Paper 95-GT-102, June 1995.

[21]Haenlein, A., "Disintegration of a Liquid Jet," NACA TN 659, 1932.

[22]Hoyt, J. W., and Taylor, J. J., "Waves on Water Jets," *Journal of Fluid Mechanics*, Vol. 83, 1977, pp. 119–127.

[23]Wu, P.-K., and Faeth, G. M., "Onset and End of Drop Formation Along the Surface of Turbulent Liquid Jets in Still Gases," *Physics of Fluids*, Vol. 7, No. 11, 1995, pp. 2915–2917.

[24]Chigier, N., and Reitz, R. D., "Regimes of Jet Breakup and Breakup Mechanisms (Physical Aspects)," *Recent Advances in Spray Combustion: Spray Atomization and Drop Burning Phenomena Volume 1*, edited by K. Kuo, Vol. 166, Progress in Astronautics and Aeronautics, AIAA, Reston, VA, 1996, pp. 109–135.

[25]Kuethe, A. M., and Chow, C.-Y., *Foundations of Aerodynamics: Bases of Aerodynamic Design*, 4th ed., Wiley, New York, 1986, p. 381.

[26]Adelberg, M., "Breakup Rate and Penetration of a Liquid Jet in a Gas Stream," *AIAA Journal*, Vol. 5, No. 8, 1967, pp. 1408–1415.

[27]Nguyen, T. T., and Karagozian, A. R., "Liquid Fuel Jets in Subsonic Crossflow," *Journal of Propulsion and Power*, Vol. 8, No. 1, 1992, pp. 21–29.

[28]Hsiang, L.-P., and Faeth, G. M., "Near-Limit Drop Deformation and Secondary Breakup," *International Journal of Multiphase Flow*, Vol. 18, No. 5, 1992, pp. 635–652.

[29]Ranger, A. A., and Nicholls, J. A., "The Aerodynamic Shattering of Liquid Drops," *AIAA Journal*, Vol. 7, No. 2, 1969, pp. 285–290.

[30]Grant, R. P., and Middleman, S., "Newtonian Jet Stability," *AIChE Journal*, Vol. 12, 1966, pp. 669–678.

[31]Chen, T.-F., and Davis, J. R., "Disintegration of a Turbulent Water Jet," *Journal of Hydraulic Division, ASCE*, Vol. 90, HY1, 1965.

G. M. Faeth
Editor-in-Chief